Intersatellite Differences of HIRS Longwave Channels Between NOAA-14 and NOAA-15 and Between NOAA-17 and METOP-A

Lei Shi

***Abstract*—Intersatellite differences of the High-Resolution Infrared Radiation Sounder (HIRS) longwave channels (channels 1–12) between National Oceanic and Atmospheric Administration 14 (NOAA-14) and NOAA-15 and between NOAA-17 and METOP-A are examined. Two sets of colocated data are incorporated in the examination. One data set is obtained during periods when equator crossing times of two satellites are very close to each other, and the data set is referred to as global simultaneous nadir overpass observation (SNO). The other data set is based on multiyear polar SNOs. The examination shows that intersatellite differences (ISDs) of temperature-sounding channels from lower stratosphere to lower troposphere, i.e., channels 3–7, are correlated with their corresponding lapse rate factors. Many of the channels also vary with respect to channel brightness temperatures; however, for the upper tropospheric temperature channel (channel 4), the patterns of ISDs from low latitudes and high latitudes are very different due to the fact that the latitudinal variation of brightness temperature does not necessarily follow the latitudinal variation of the temperature lapse rate. The differences between observations in low latitudes and high latitudes form "fork" patterns in scatter plots of ISDs with respect to brightness temperatures. A comparison of ISDs derived from short-term global SNOs and those derived from multiyear polar SNOs reveals the advantage and the limitation of the two data sets. The multiyear polar SNO generally provides larger observation ranges of brightness temperatures in channels 1–4. The global SNO extends the brightness temperature observations to the warm sides for channels 5–12 and captures the occurrences of larger ISDs for most longwave channels.**

***Index Terms*—Infrared sounder, intercalibration, remote sensing, simultaneous nadir overpass observations (SNOs).**

I. Introduction

THE High-Resolution Infrared Radiation Sounder (HIRS) instruments have been onboard the Television Infrared Observation Satellite (TIROS-N) and the National Oceanic and Atmospheric Administration (NOAA) polar orbiting satellite series (hereafter abbreviated as N#, where # is the satellite number) since 1978 and more recently on the Meteorological Operational Satellite Program (METOP). However, due to the spectral differences of the HIRS instruments and the independent calibration of each instrument's measurement, transitions between satellites have created intersatellite biases. These biases are an obstacle in using the aggregated long-term time series for climate studies. Various attempts have been made in recent years to quantify the biases. Using an empirical analysis assuming that the statistical distributions of anomalies from same targets observed by two satellites are the same, Bates *et al.* [1] intercalibrated 13 years of HIRS channel-12 data from 1981 to 1993. Based on polar simultaneous nadir overpass observations (SNOs), Cao *et al.* [2] compared the radiances of the 19 HIRS infrared channels on boards N15, N16, and N17, and Shi *et al.* [3] depicted scene radiance-dependent HIRS longwave channel biases from N06 to N17. Using the Atmospheric Infrared Sounder (AIRS) observations, Wang *et al.* [4] assessed NOAA-16 HIRS's radiance accuracy. Compared with the Infrared Atmospheric Sounding Interferometer (IASI) observations, Cao *et al.* [5] calculated radiances from HIRS instruments to separate intersatellite biases induced by spectral response functions. Based on zonal means of every ten latitude belts of overlapping satellites, Shi and Bates [6] showed intersatellite biases of clear-sky HIRS channel 12 between pairs of satellites from the TIROS-N to the METOP-A (hereafter abbreviated as M02). More activities are ongoing as part of the Global Space-based Intercalibration System [7]. This paper joins the effort with observational records from both polar and global SNOs.

Due to the orbital drift associated with each NOAA satellite, there were brief periods of time when two satellite orbits overlap each other. Recent overlapping orbits occurred in satellite pairs N14 and N15 in 2003, N15 and N16 in 2008, N17 and M02 in spring 2009, and N18 and N19 in fall 2009. A description of overlapping orbits and their application in intercalibrating microwave humidity sounders can be found in [8]. The overlapping orbits present an opportunity to examine intersatellite biases when the satellites measure same targets in a global scale. This includes low-latitude observations that are not covered by polar SNOs in previous HIRS studies.

This paper examines intersatellite differences (ISDs) of colocated observations from two satellite pairs: N14 and N15, and N17 and M02. These two pairs represent the transitions from HIRS/2 instrument design to HIRS/3 design and from HIRS/3 to HIRS/4 design, respectively. N16 is not selected for this paper due to significant degradation experienced by the instrument in 2008, and N18 HIRS is not selected due to instrument problems in 2009. The HIRS sensor status is recorded and provided online by the NOAA Office of Satellite Operations at http://www.oso.noaa.gov/poesstatus/. HIRS on N16 degradation began in summer 2004 and became worsen in later years. HIRS data on N18 since February 2009 were described by the NOAA Office of Satellite Operations as "degraded and unusable for the user community."

Manuscript received December 30, 2011; revised April 11, 2012 and July 9, 2012; accepted July 21, 2012. Date of publication October 18, 2012; date of current version February 21, 2013.

The author is with the National Oceanic and Atmospheric Administration/National Environmental Satellite, Data, and Information Service/National Climatic Data Center, Asheville, NC 28801 USA (e-mail: Lei.Shi@noaa.gov).

Digital Object Identifier 10.1109/TGRS.2012.2216886

U.S. Government work not protected by U.S. copyright.

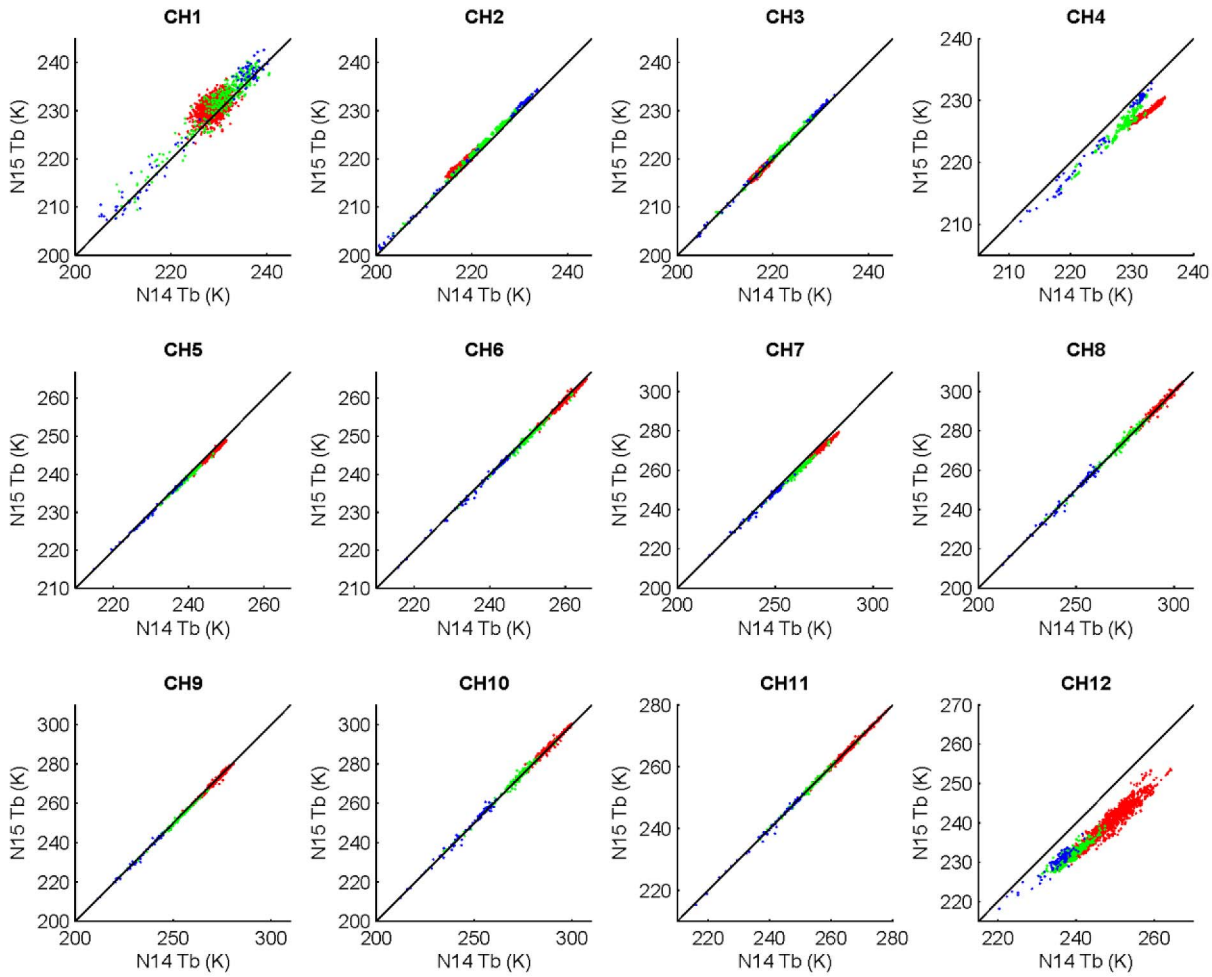

Fig. 1. Scatter plots of Tb observations for channels 1–12 between N14 and N15. Red, green, and blue denote observations from low (below 40°), mid- (40°–70°), and high (above 70°) latitudes, respectively. Unity lines are drawn to facilitate comparisons.

The HIRS instrument has 20 channels. Channels 1–12 are longwave channels with center wavenumbers in the range of 665 to 1530 cm^{-1}. Channels 13–19 are shortwave channels in the wave spectra between 2100 and 2700 cm^{-1}. Channel 20 is a visible channel. In this paper, the ISD of HIRS instruments on different satellites is examined for each of the longwave channels 1–12. These are primary channels used for deriving temperature [9], [10], humidity [10], surface emissivity [11], cloud property [12]–[14], and outgoing longwave radiation [15], and those used as validation for newly developed sounder data [16]. The examination starts with a comparison of brightness temperature (Tb) observations from globally colocated data during satellite orbit overlapping periods. The differences between ISDs derived from global and polar SNOs are then shown. The effect of vertical-temperature lapse rate on ISDs is explored. The aim is to use an observational-based data set to facilitate intersatellite calibration efforts.

II. ISDs

A. Comparison of Tb Observations From Global SNO

N14 was launched in December 1994 as an afternoon satellite, and N15 was launched in December 1998 as a morning satellite. Through the years, N14 and N15 drifted in opposite directions. In 2003, the orbits of N14 and N15 were very close to each other. For a short period in April–May 2003 (Julian Days 102–129 in 2003), the equator crossing times of the two orbits were within 2 min. Data during this overlapping period are processed. To reduce uncertainties associated with the presence of clouds, clear-sky pixels are chosen in this paper. There are 56 pixels in each HIRS scan line. To minimize limb-viewing effects, pixels from the center four positions (positions 27–30) within 2 min of observation time are colocated. In the colocation processing, only clear-sky pixels having more than half of the overlapping footprints are selected. The cloud detection used an approach similar to the International Satellite Cloud Climatology Project algorithm [17]. The method combined both spatial and temporal variations in brightness temperatures as described in [18]. The space and time tests for detecting clouds followed the logical tables in [17]. The data cover all latitudes and over both land and water surfaces. Fig. 1 shows the scatter plots of N14 and N15 brightness temperatures for channels 1–12. There are a total of 1772 colocated points. In the plots, data from low (less than 40°), mid- (between 40° and 70°), and high (greater than 70°) latitudes are colored in red, green, and blue, respectively. Data's mean and standard deviation (STD) values, as well as correlations between the two satellite observations, are listed in Table I. As expected, most of the corresponding channels closely relate to each other. The correlation coefficients are greater than 0.9

TABLE I
STATISTICS FOR N14 TB MEAN, N15 TB MEAN, N14 TB STD, N15 TB STD, CORRELATION COEFFICIENT BETWEEN N14 TB AND N15 TB, MEAN ISD BETWEEN N14 AND N15, STD OF ISD BETWEEN N14 AND N15, AND CORRELATION COEFFICIENT BETWEEN N14 TB AND N14-N15 ISD. DATA ARE DERIVED FROM THE PERIOD WHEN THE EQUATOR CROSSING TIMES OF THE TWO SATELLITES ARE CLOSE TO EACH OTHER

Channel	N14 Mean	N15 Mean	N14 STD	N15 STD	N14&N15 Tb Correlation	ISD Mean	ISD STD	Tb&ISD Correlation
1	228.97	230.71	4.23	4.25	0.904	-1.74	1.85	0.208
2	218.52	219.36	4.34	4.28	0.995	-0.85	0.42	0.187
3	218.25	218.36	3.80	3.92	0.997	-0.10	0.31	-0.353
4	232.11	228.09	2.93	2.35	0.931	4.02	1.14	0.658
5	244.67	243.88	5.10	4.92	0.999	0.79	0.26	0.681
6	257.45	256.94	7.31	7.26	0.999	0.51	0.26	0.206
7	270.61	268.11	9.77	9.24	0.999	2.50	0.67	0.796
8	287.25	287.32	13.95	13.94	0.999	-0.06	0.64	0.051
9	266.80	266.33	12.62	12.58	0.999	0.47	0.41	0.099
10	283.14	283.46	12.59	12.61	0.999	-0.32	0.61	-0.017
11	262.10	261.99	7.82	7.81	0.999	0.11	0.30	0.056
12	246.01	237.94	6.77	5.77	0.971	8.07	1.81	0.645

for all channels. However, larger scatterings are observed for channels 1, 4, and 12. The larger scattering feature in channel 1 is in part due to its significant noise equivalent differential radiance (NEΔN). According to the "NOAA Polar Orbiter Data User's Guide" (available at http://www.ncdc.noaa.gov/oa/pod-guide/ncdc/docs/podug/index.htm) and the "NOAA KLM User's Guide" (available at http://www.ncdc.noaa.gov/oa/pod-guide/ncdc/docs/klm/index.htm), channel 1's NEΔN value is 3.00 mW/$(\mathrm{m}^2 \cdot \mathrm{sr} \cdot \mathrm{cm}^{-1})$, a value much larger than other channels. The NEΔN values are 0.67 and 0.50 mW/$(\mathrm{m}^2 \cdot \mathrm{sr} \cdot \mathrm{cm}^{-1})$ for channels 2 and 3, respectively, and less than or equal to 0.31 mW/$(\mathrm{m}^2 \cdot \mathrm{sr} \cdot \mathrm{cm}^{-1})$ for all other infrared channels. As a result, the measurements from channel 1 are much noisier than other channels.

For channel 4, the data fork near and above the value of 230 K. It is interesting to note that the fork pattern is composed of data from mostly low latitudes in the lower branch and from high and midlatitudes (mostly from latitudes higher than 60°) in the upper branch. This exhibits significant differences in ISDs between low and high latitudes. In the HIRS sounder design, central frequencies for temperature-sounding channels are selected along the sharp absorption line of carbon dioxide between 665–750 cm^{-1} (see Fig. 1 in [3]) to observe the atmosphere at altitudes from the surface to stratosphere. Because of the difference in channel response functions between channel 4 on N14 and channel 4 on N15, the two instruments observe the atmosphere through slightly different carbon dioxide absorptions, and thus, they observe temperatures at slightly different heights (hereafter, $\Delta H_{\Delta\mathrm{sat}}$ is used to denote the difference of measurement heights from the same channel on different satellites). If there is temperature difference in $\Delta H_{\Delta\mathrm{sat}}$, there is difference in Tb measurements of the instruments from two satellites (i.e., ISD). The ISD represents a measure of the atmospheric vertical-temperature lapse rate between two slightly different heights.

As different HIRS channels observe Tb at different altitudes, the measurements between two adjacent temperature-sounding channels provide a mean to estimate the significance of temperature difference between $\Delta H_{\Delta\mathrm{sat}}$. Among the suite of HIRS temperature-sounding channels, channel 4 measures the temperature in the upper troposphere, whereas channel 5 measures the temperature in the midtroposphere. The difference of these two channels represents the vertical-temperature difference between mid- and upper tropospheres. Although the measurement height difference between channels 5 and 4 is much larger than $\Delta H_{\Delta\mathrm{sat}}$, the Tb difference between channels 5 and 4 can be an indication of how large the Tb difference is in $\Delta H_{\Delta\mathrm{sat}}$. The distributions of N14 channel-4 Tb and the Tb difference between channels 5 and 4 with respect to latitude are shown in the upper and lower left panels in Fig. 2. These are from the same global colocated observations plotted in Fig. 1. The top left panel in Fig. 2 shows that, over low latitudes of less than 40°, channel 4's Tb values are generally greater than 230 K. During the N14

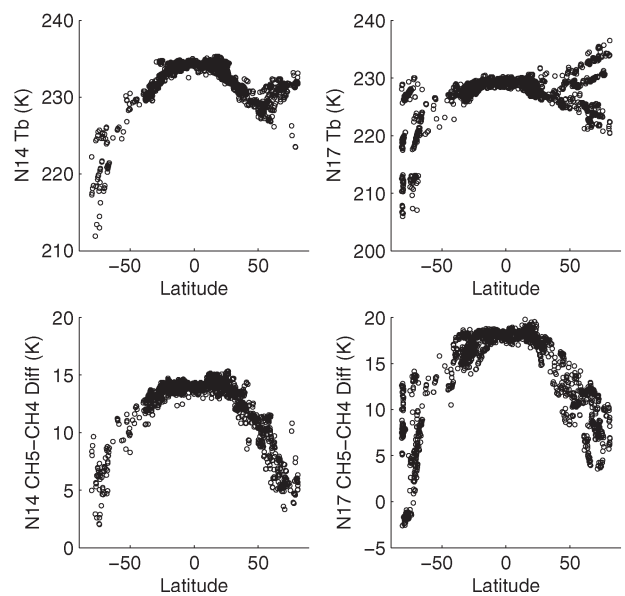

Fig. 2. Variations of (upper two panels) observed channel-4 Tb values and (lower panels) Tb differences between channels 5 and 4 for N14 and N17.

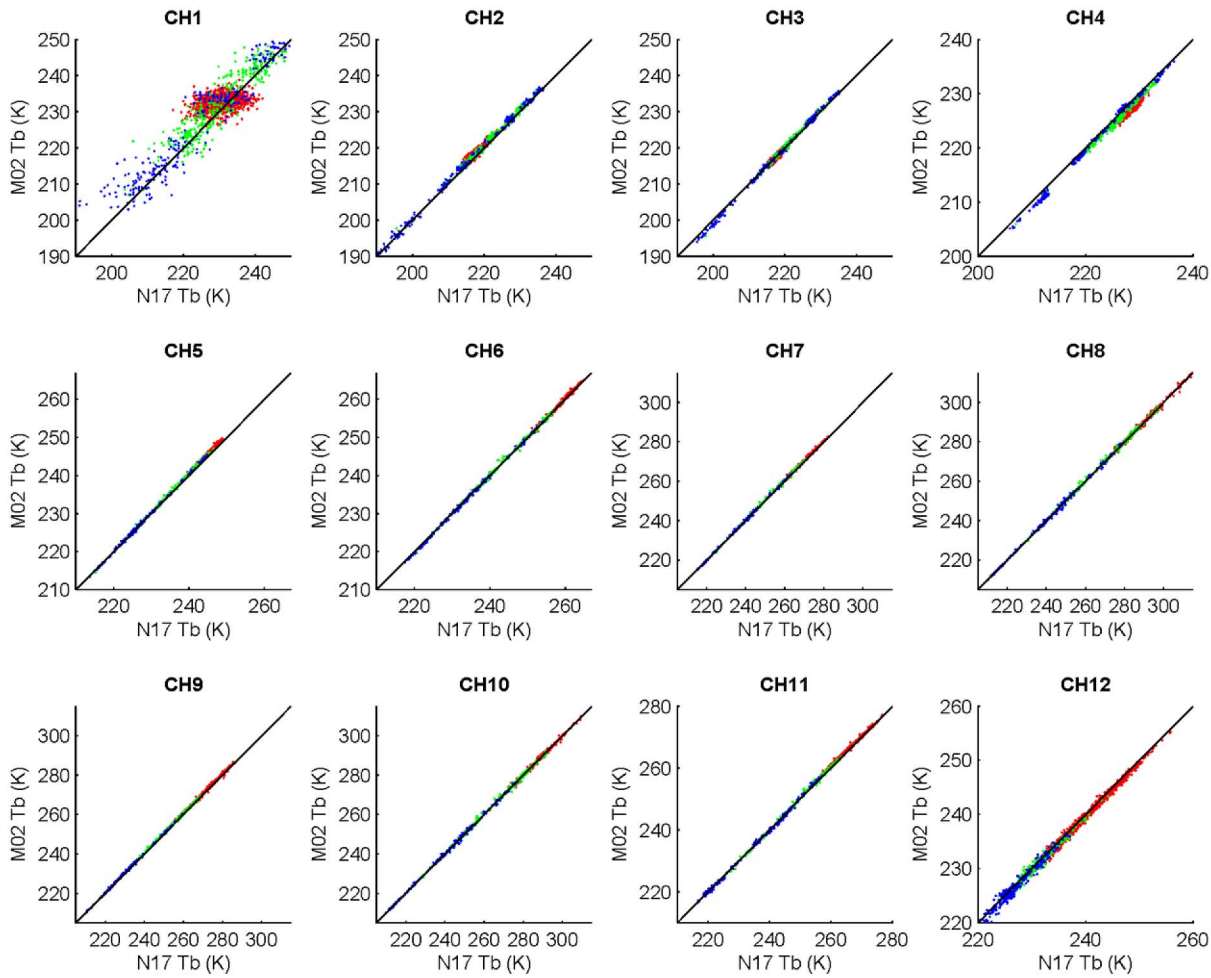

Fig. 3. Same as Fig. 1 except for satellites N17 and M02.

and N15 orbital overlapping period in the spring time, the Tb observations over southern high latitudes are low (generally less than 225 K); however, over the northern high latitudes, the Tb values can be greater than 230 K. From the lower left panel in Fig. 2, the Tb difference between channels 5 and 4 is largest over low latitudes. This shows that the vertical-temperature lapse rates in low latitudes are large. The lapse rates significantly decrease over high latitudes. Associated with large lapse rates in low latitudes, Tb observations more significantly deviate from the unity line in Fig. 1 and form the lower branch in the channel-4 fork. The similarly high Tb values observed in northern high latitudes are associated with smaller lapse rates; therefore, the Tb observations are not affected as much as those in low latitudes. These large Tb values in high latitudes form the upper branch of the channel 4 fork in Fig. 1.

Scatter plots for Tb between N17 and M02 are shown in Fig. 3. The data are taken from Julian Days between 66 and 185 in 2009 when the equator crossing times of N17 and M02 were very close to each other. Similar to the N14–N15 pair, only clear-sky pixels in the center four positions of scan lines and within 2 min of global observations are colocated. The HIRS pixel size of M02 (∼10 km) is much smaller than that of N17 (∼20 km). In the colocation, only M02 pixels within N17 footprints are selected. There are a total of 1804 colocated points during this period. The statistics of this data set is listed in Table II. Also, as expected, most of the channels tightly relate to each other. Among the 12 channels, channel 1 displays largest scattering between the two satellites. As shown in Table II, all the channels except channel 1 have linear correlation coefficients of greater than 0.99. For channel 4, the colocated points from low latitudes display more deviation from the unity line than those from high latitudes of the same Tb range. More details of ISDs are shown in the next section.

B. Relationship Between ISD and TB

To further illustrate ISD, Fig. 4 presents scatter plots of the ISD between N14 and N15 with respect to N14 Tb. The ISD is calculated by subtracting N15 Tb from N14 Tb. The red, green, and blue plots show the colocated global SNO data from low, mid-, and high latitudes, respectively, during Julian Days 102–129 of 2003. These are from the same observations plotted in Fig. 1. The term "global SNO" is used here to refer to colocated data during the short periods when two satellites' equator crossing times are within 2 min. There are additional plots (in cyan) taken from multiyear polar SNO data presented in [3]. The term "polar SNO" refers to colocated data taken from a period of several years from latitudes higher than 70°. Procedures for obtaining polar SNOs are described in detail in [19] and [2]. The polar SNOs occur when two satellites intersect

TABLE II
STATISTICS FOR N17 TB MEAN, M02 TB MEAN, N17 TB STD, M02 TB STD, CORRELATION COEFFICIENT BETWEEN N17 TB AND M02 TB, MEAN ISD BETWEEN N17 AND M02, STD OF ISD BETWEEN N17 AND M02, AND CORRELATION COEFFICIENT BETWEEN N17 TB AND N17–M02 ISD. DATA ARE DERIVED FROM THE PERIOD WHEN THE EQUATOR CROSSING TIMES OF THE TWO SATELLITES ARE CLOSE TO EACH OTHER

Channel	N17 Mean	M02 Mean	N17 STD	M02 STD	N17&M02 Tb Correlation	ISD Mean	ISD STD	Tb&ISD Correlation
1	229.59	231.38	8.10	7.43	0.892	-1.79	3.67	0.401
2	218.01	218.84	6.42	6.41	0.995	-0.83	0.65	0.064
3	218.28	218.18	5.47	5.74	0.997	0.10	0.51	-0.494
4	227.18	225.89	4.20	4.06	0.990	1.29	0.61	0.298
5	241.56	242.16	7.91	8.17	1.000	-0.60	0.34	-0.769
6	252.99	253.09	11.62	11.80	1.000	-0.10	0.30	-0.567
7	262.84	263.17	15.44	15.58	1.000	-0.33	0.36	-0.394
8	280.04	280.08	23.31	23.36	1.000	-0.04	0.51	-0.074
9	261.10	261.62	18.36	18.49	1.000	-0.52	0.36	-0.355
10	276.55	276.51	21.49	21.41	1.000	0.04	0.47	0.185
11	258.25	258.49	12.80	12.93	1.000	-0.25	0.42	-0.308
12	235.94	235.55	6.68	6.64	0.997	0.39	0.52	0.112

in 70°–80° latitudes due to the orbital nature of the NOAA series of polar orbiting satellites. The N14 and N15 polar SNO data examined in this paper cover the period from 1999 to 2003, containing 377 colocated data points.

Fig. 4 shows that for channel 1, the multiyear polar SNO and short-term global SNO are in different patterns. The majority of polar SNO plots are between −3 and 0 K across the entire Tb range, but the low and midlatitude SNOs show a sharply upward slope of the ISD with increasing Tb in the range of 220–240 K. The ISD from global SNO ranges from −7 to over 3 K, but the ISDs from the polar SNO are limited to a narrower range of values. The difference in these two patterns is an exhibition of the limitations from both data sets. For the polar SNO, due to its polar restriction, the data do not cover the measurements in mid- and low latitudes. The large negative ISD (−7 K) and the large positive ISD (3 K) obtained from the global SNO are not captured by the polar SNO. On the other hand, the global matchups from a short period do not have sufficient data to cover the very cold (200 K) and very warm (250 K) Tb observations from other seasons. Due to large temporal temperature variations in polar regions, including seasonal changes, along with more dramatic changes such as sudden stratospheric warming [20]–[22], polar jets, and frequent polar lows (e.g., [23]), the multiyear polar SNO covers a much larger Tb observation range.

For channels 2 and 3, the plots from both global and polar data sets mostly fall in the same ranges of ISDs; however, near the medium ranges of the observed Tb, there are indications of larger absolute values of ISDs in global SNOs than in polar SNOs. Channel-2 ISDs spread in the range of −2–0.5 K. Channel-3 ISDs are mostly in the range of −1–1 K, with slightly increasing negative ISD with respect to Tb.

For channel 4, the ISD patterns from global and polar SNOs are remarkably different. ISDs from the polar SNO follow a gradually decreasing pattern, in average from 3 to 0 K from Tb observations of 210 to 235 K. For the global SNO plot in the Tb range of 230–240 K, there is clearly a branch of increasing ISD (3 to 5.5 K) that is not captured by the polar SNO. This branch is composed of observations mostly from low latitudes and is the same observation of the lower branch of the channel-4 fork featured in Fig. 1. Large values of channel-4 Tb can be observed in both low and high latitudes, but the ISDs are much more significant for low-latitude observations due to the larger vertical-temperature lapse rate there.

For channels 5–12, multiyear polar SNOs share very similar ISD patterns as those of short-term global SNO data in low-to-medium temperature ranges. For channels 5 and 6, the ISDs between N14 and N15 increase with respect to Tb, from −0.5 to 1.5 K for channel 5, and from near zero to above 0.5 K for channel 6. Channel 7 is at the sharp slope of the absorption line. Even small changes in channel frequencies can lead to large differences in satellite observations. Channel-7 ISDs can be as large as 4 K at the observing Tb of 280 K as revealed in global SNOs, but polar SNOs can only show ISD as large as 2 K at Tb of 260 K. The polar SNOs cannot capture the full extents of ISDs in high Tb observations. The averages of ISDs for channels 8, 10, and 11 are relatively small. For channel 9, the ISD increases from 0 to 0.5 K as a function of Tb.

Among all longwave channels, channel 12 exhibits the largest variation of the ISD across Tb observations. The large ISD value in channel 12 is due to the channel frequency change from 1481 cm^{-1} in HIRS/2 design on N14 to 1530 cm^{-1} in HIRS/3 design on N15. There is a large difference in measured top-value ISDs between global and polar SNOs. The global ISD can reach 12 K, a value much larger than what is covered by the polar SNO. Similar scatter plot features can be also found in [24] for monthly radiance differences between N14 and N15 when channel-12 measurements are compared using colocated geostationary data as references. In the cold Tb observation of less than 220 K in channel 12, the multiyear polar SNO shows negative ISDs that are not observed during the short-term global SNO.

The ISD plots between N17 and M02 for the 12 longwave channels are displayed in Fig. 5. The ISD is calculated by subtracting M02 Tb from N17 Tb. The red, green, and blue points are global data taken from 2009 when the equator

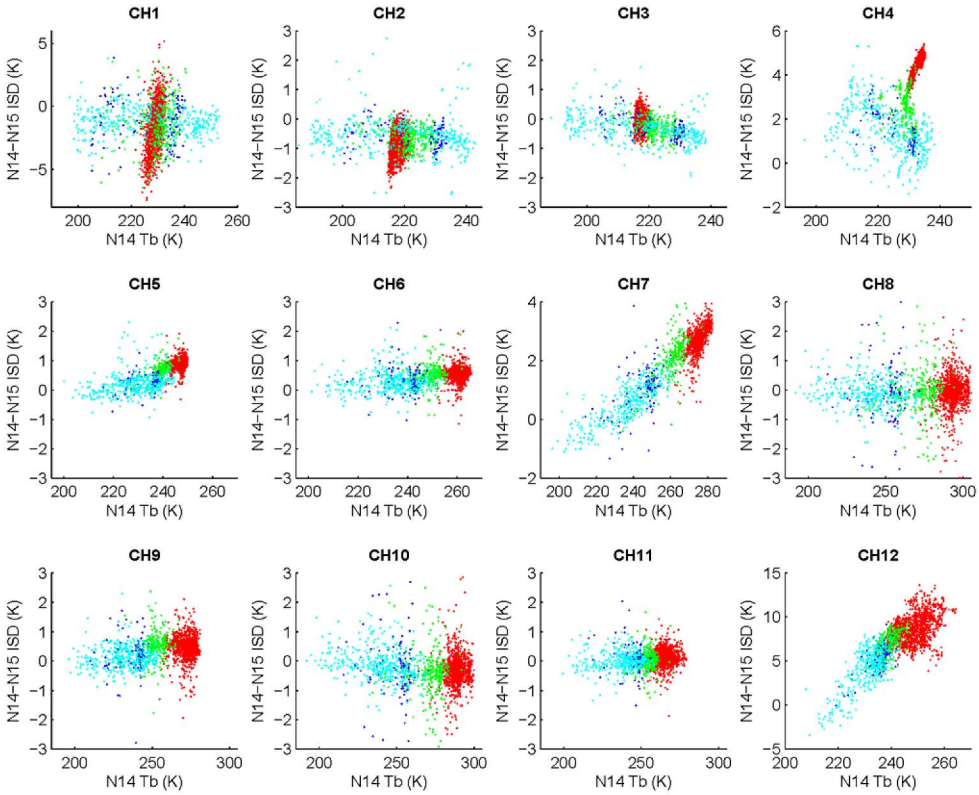

Fig. 4. ISDs between N14 and N15 for channels 1–12. Red, green, and blue represent ISDs of low, mid-, and high latitudes, respectively, from the short-term global SNO, and cyan represents ISDs from the multiyear polar SNO.

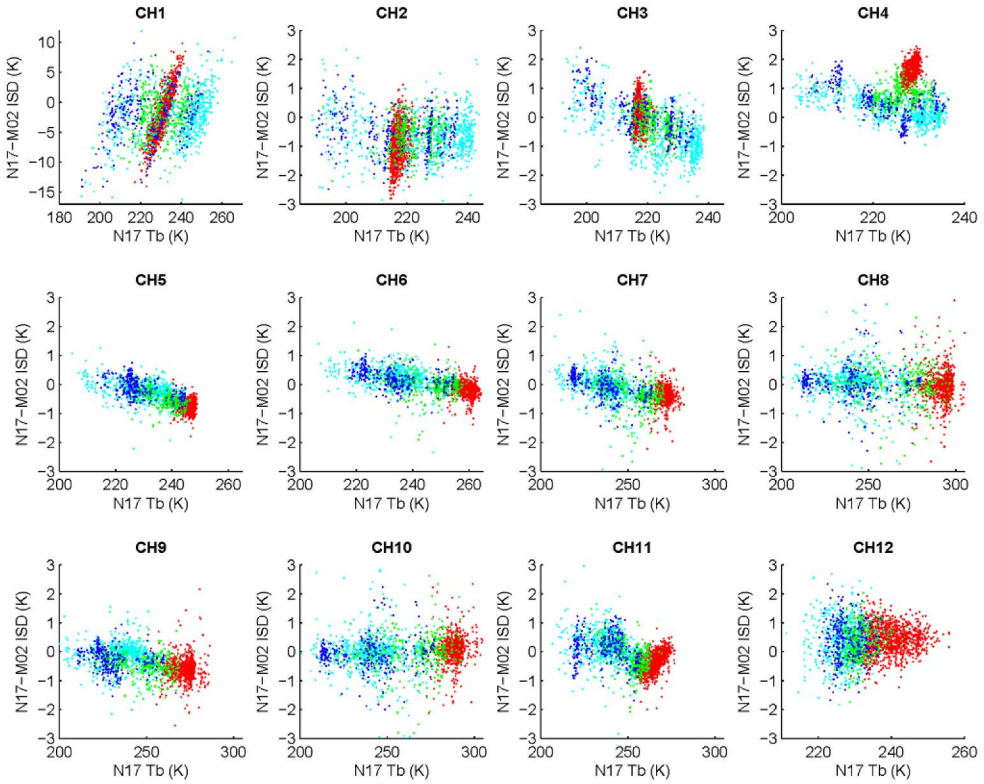

Fig. 5. Same as Fig. 4 except for the ISDs between N17 and M02.

crossing times of N17 and M02 were very close to each other, and these are the same observations presented in Fig. 3. The cyan points in Fig. 5 are taken from the 2008–2011 colocated pixels of polar SNOs (containing 935 colocated data points). Fig. 5 shows that, for the stratospheric channels in the carbon dioxide band (channels 1–3), the short-term global SNO plots

mostly appear to be a subset of multiyear polar SNO plots. However, in certain ranges of Tb observations, the global SNOs display larger ISDs that are not in polar SNOs. For example, at a Tb value of 240 K in channel 1, the low-latitude SNO data show an ISD of 7–8 K, and at a Tb value of 215 K in channel 2, the low-latitude SNO data show an ISD of -2.8 K. In both cases, the absolute values of ISDs from global SNOs are larger than ISDs from polar SNOs at the same Tb observations. For channels 1–3, the multiyear polar SNOs have larger coverage of Tb observations than the global SNOs. Although there was a significant sudden stratospheric warming event in January of 2009 [25], [26], the warming event was outside of the global orbit overlapping window of N17 and M02, and thus, the large temperature change was not observed in the global SNO. Among all the 12 longwave channels, channel 1 exhibits the largest variation of ISD between N17 and M02, with ISD values ranging from -15 to 8 K. Consistently large ISDs for HIRS channel 1 were also noted in many of other NOAA series of satellites [2], [3]. For channel 2, the averaged ISDs are around -1 K; however, the ISDs can considerably vary from -2.8 to 1 K. For channel 3, there is a trend of decreasing ISD values from an average of 1 K to an average of -1 K with respect to Tb observations.

An interesting feature similar to the N14–N15 pair appears in channel 4 near 230 K. Around this value, the N17–M02 ISDs from low-latitude SNOs are much larger (with peak at 2.5 K) than the ISDs from polar SNOs. As shown in the lower right panel in Fig. 2, the Tb difference between channels 5 and 4 is the largest in low latitudes. The Tb measurement differences between N17 and M02 are therefore affected more by the larger vertical-temperature lapse rate there. Tb values of 230 K and higher are also observed in the northern high latitudes (as shown in the upper right panel in Fig. 2). However, these measurements are associated with much smaller values of vertical-temperature lapse rates, and their ISDs are affected less compared with low-latitude observations. Some negative ISD values are shown from global SNO data around the Tb value of 227 K. Most of these data are associated with negative difference values between channels 5 and 4 (indicating deep temperature inversion) over the Antarctica as displayed in the lower right panel in Fig. 2. Overall, the channel-4 ISDs vary in the range of -0.8–2.5 K.

For channels 5–12, the ISD patterns from global SNOs are basically extensions of the polar ISD patterns in the warm ends of Tb observations. These extensions are essential in obtaining the full range of ISD variations. For example, in warm Tb observations, the ISDs of -0.5 to -1 K in channels 5, 6, 7, 9, and 11 all contribute to establishing the lower bounds of the ISD range values. For these channels, the overall (combining both global and polar SNOs) ISDs vary more than 0.5 K from the cold to warm Tb measurements, and thus, it is important to have data from both low and high Tb observations. For channel 11 in the Tb observation range of 240–270 K, the scatter plot displays a nonlinear feature of the ISD pattern. This nonlinear feature should be considered in intersatellite calibration.

C. Relationship Between ISD and LRF

Previous sections illustrated strong relationship between ISD and vertical-temperature difference for channel 4. Discussions about the influence of the lapse rate on the ISD can be also found in [2], which showed that the intersatellite radiance bias of channel 3 strongly correlates with the radiance difference between channels 3 and 2. A term "LRF" was used in [2] to represent the radiance difference between channels 3 and 2. Borrowing this term, the "LRF" is used here to refer to the Tb difference between channels sensing adjacent vertical layers. The correlation between the LRF and the ISD is the largest for channels that measure atmospheric layers with a large lapse rate and for channels that the spectral response functions between two HIRS instruments significantly differ. Thus, a low correlation (and a low STD of the difference) between the ISD and the lapse rate could either mean that two HIRS instruments are very similar in their spectral responses or that the LRF does not represent temperature difference between $\Delta H_{\Delta\mathrm{sat}}$ well. Fig. 6 displays the relationships between LRFs and ISDs of channels 1–7 for the N14–N15 pair. Channels 1–7 are atmospheric-temperature-sounding channels from the stratosphere to near surface. The red, green, and blue plots are the same short-term global observations presented in Fig. 1, and the cyan plots are the same multiyear polar observations showed in Fig. 4.

Fig. 6 shows that, for channel 1, when combining both global and polar SNOs, there is no apparent relationship between the LRF and the ISD. For channel 2, the ISD from the global SNO shows a very different pattern from the polar SNO. The polar data have larger ranges of LRFs from the multiyear observation.

For channels 3 and 4, there are good alignments of polar ISDs and global ISDs in the plots. For channel 3, the global ISD plots almost overlap with the polar ISD plots, and for channel 4, the plots from the two SNO sources are also close to each other. There is a large variation of the ISD for channel 4 from -1.5 to 5.5 K as a function of the LRF.

For channels 5–7, the variations of ISDs are also correlated with their LRFs. The plot patterns are similar to the patterns displayed in Fig. 4 for channels 5–7. Channels 5 and 6 observe the mid- and lower troposphere, respectively, and channel 7 observes the near-surface air temperature. In these layers, the lapse rate is closely related to Tb; thus, the ISDs of channels 5–7 vary with the LRF in similar patterns as with Tb. Globally, high temperatures of these layers are typically found in tropics, and low temperatures are located in polar regions. The latitudinal distributions of their LRFs are also relatively large in low latitudes and relatively small in high latitudes. The sensors from two satellites measure larger differences in Tb values where the vertical-temperature lapse rate is greater. Therefore, ISDs of these channels increase with Tb and are more significant in low latitudes.

Table III lists the statistics of the LRFs and ISDs calculated based on N14 and N15 short-term global SNO, multiyear polar SNO, and combined global and polar SNO data for channels 1–7. In the table, the term "All" is used to denote all available data from both global and polar SNOs. Although linear correlation coefficients are calculated for these variables to facilitate the analysis, it does not necessarily suggest using linear regression fit to intercalibrate each of these channels. As discussed below, a linear regression fit may not work well for some of the channels between certain satellite pairs.

For channel 1, the correlation coefficients from global and polar SNO data are in opposite signs with low correlation values. Combining both global and polar SNO data, the correlation coefficient for channel 1 is closed to zero, indicating

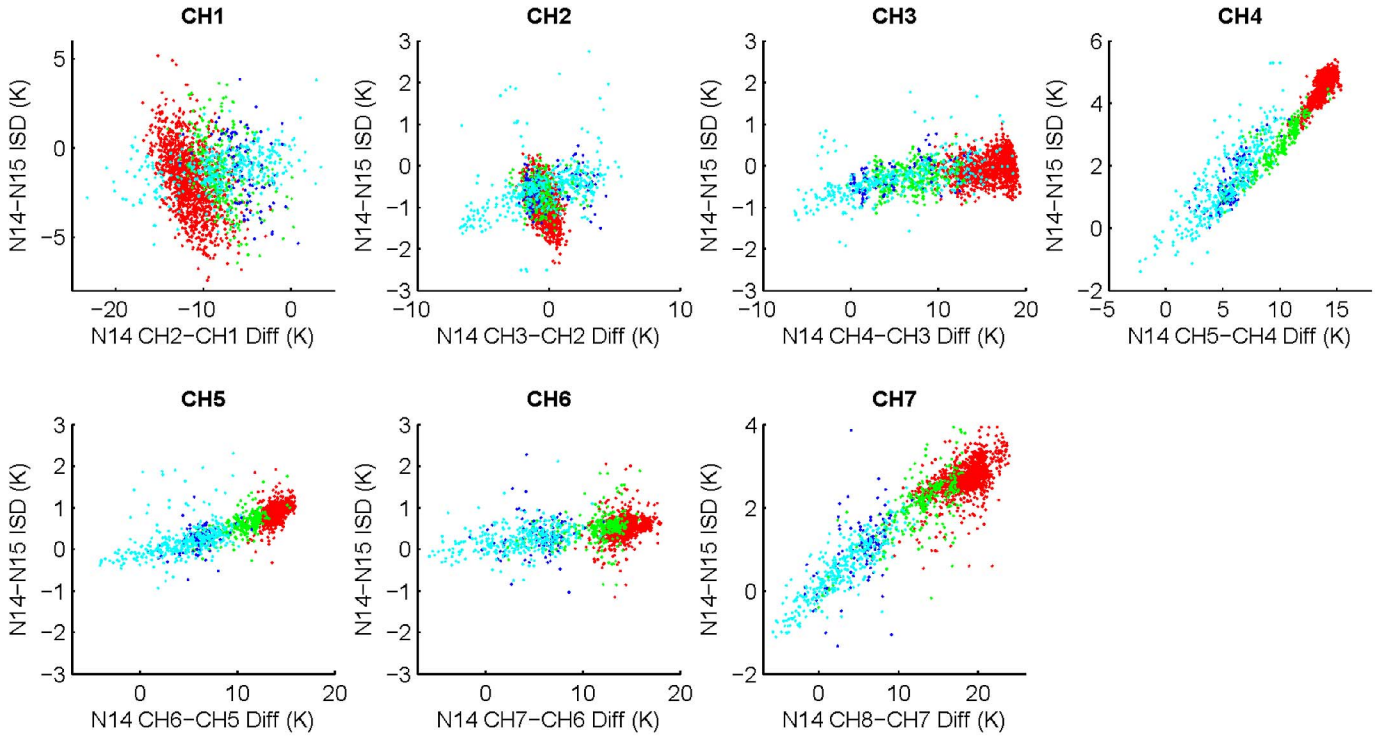

Fig. 6. ISD between N14 and N15 plotted as a function of respective LRF. Red, green, and blue represent ISDs of low, mid, and high latitudes, respectively, from the short-term global SNO, and cyan represents ISDs from the multiyear polar SNO.

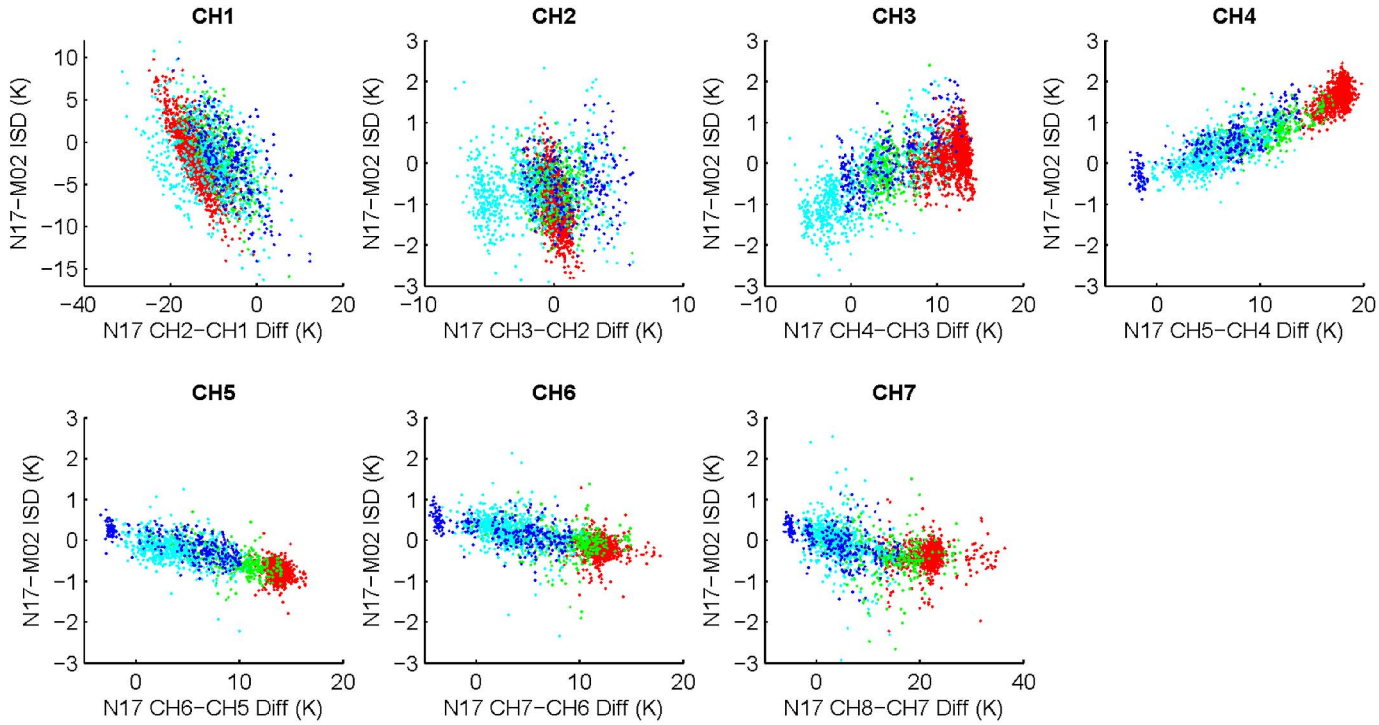

Fig. 7. Same as Fig. 6 except for ISD between N17 and M02.

uncertainty in the relationship between the LRF and the ISD. As the STD of the ISD is large, a small value of correlation implies that the lapse factor is not a good representation of the temperature difference in $\Delta H_{\Delta\mathrm{sat}}$ for this layer, likely due to the fact that the lapse rate between measurement heights of channels 1 and 2 and the lapse rate between $\Delta H_{\Delta\mathrm{sat}}$ of channel 1 are very different. The large NEΔN value of channel 1 also contributes to the spread of the ISD and small correlation values. For channel 2, the correlation coefficients derived from the polar SNO are about twice as large as that derived from the global SNO but in opposite signs. Data from the short-time global SNO cover only a fraction of the Tb range observed by the multiyear polar SNO and may not be sufficient to derive the correlation relationship for other seasons. For channel 3,

TABLE III
STATISTICS FOR MEAN OF N14-N15 ISD, MEAN OF N14 LRF, STD OF N14-N15 ISD, STD OF LRF, AND THE LINEAR CORRELATION COEFFICIENT BETWEEN LRF AND N14-N15 ISD CALCULATED BASED ON N14 AND N15 SHORT-TERM GLOBAL SNO, MULTIYEAR POLAR SNO, AND COMBINED GLOBAL AND POLAR SNO (LABELED AS "ALL") DATA FOR CHANNELS 1–7

	Channel	LRF	ISD Mean	LRF Mean	ISD STD	LRF STD	Correlation
Short-term Global	1	CH2-CH1	-1.74	-10.45	1.85	2.90	-0.243
	2	CH3-CH2	-0.85	-0.26	0.42	0.87	-0.228
	3	CH4-CH3	-0.10	13.86	0.31	4.90	0.391
	4	CH5-CH4	4.02	12.56	1.14	2.61	0.963
	5	CH6-CH5	0.79	12.78	0.26	2.42	0.754
	6	CH7-CH6	0.51	13.16	0.26	2.70	0.297
	7	CH8-CH7	2.50	16.65	0.67	4.45	0.795
Multi-year Polar	1	CH2-CH1	-1.22	-7.90	1.10	4.82	0.361
	2	CH3-CH2	-0.54	-0.42	0.62	2.78	0.411
	3	CH4-CH3	-0.32	4.95	0.47	5.77	0.563
	4	CH5-CH4	1.45	5.27	1.08	2.48	0.830
	5	CH6-CH5	0.21	4.60	0.40	3.09	0.412
	6	CH7-CH6	0.24	3.67	0.30	3.53	0.351
	7	CH8-CH7	0.57	3.03	0.73	3.87	0.839
All	1	CH2-CH1	-1.49	-9.17	1.89	4.60	0.098
	2	CH3-CH2	-0.73	-0.27	0.51	1.15	-0.007
	3	CH4-CH3	-0.12	11.72	0.33	6.87	0.305
	4	CH5-CH4	3.39	10.66	1.78	4.95	0.976
	5	CH6-CH5	0.66	10.85	0.39	4.92	0.870
	6	CH7-CH6	0.45	11.19	0.30	5.21	0.495
	7	CH8-CH7	2.11	13.98	1.08	7.40	0.922

the correlation between the LRF and the ISD becomes clear with a larger coefficient from polar SNO data. The largest correlation coefficient is found in channel 4. Based on all available data from both global and polar SNOs, the correlation coefficient between the LRF and the ISD for channel 4 is as large as 0.98. Channels 5 and 7 also have relatively large correlation coefficients. For channel 6, although the correlation is not as high as channels 4, 5, and 7 in short-term global data and multiyear polar data, the correlation coefficient can be as large as 0.50 when data from both SNO sources are combined.

Similar to Fig. 6, Fig. 7 shows scatter plots between ISDs and LRFs of channels 1–7 between N17 and M02. Again, no clear relationship between the ISD and the LRF is observed for channel 1. The polar ISD of channel 2 appears to display a slight dependence of the ISD on the LRF. Similar to the N14–N15 pair, both global and polar SNOs of channels 3 and 4 display high dependences of ISDs on the LRF for the N17–M02 pair. In the examination of intersatellite radiance biases on N15, N16, and N17 from polar SNOs, Cao *et al.* [2] discussed that the seasonal bias variation in the stratosphere channels is highly correlated with the LRF approximated by the channel radiance differences. This paper on the N14–N15 and N17–M02 pairs shows that channel 3 is highly correlated with the LRF, as presented in [2], but the result for the other two tropospheric channels, particularly for channel 1, is not conclusive. This paper also shows that the ISD of the upper tropospheric temperature channel, i.e., channel 4, is highly correlated with its LRF. The ISDs of the mid- to low-tropospheric temperature channels 5–7 are also found correlated to their LRFs, although their ISDs can be as well viewed as Tb dependent (see Figs. 4 and 5).

The linear correlation coefficients between ISDs and LRFs of channels 1–7, along with other statistics for N17 and M02 are listed in Table IV. For channel 1, data from global and polar SNOs both result in negative correlation coefficients; however, the correlation values could be overestimated by the distributions of endpoints in both sides of the lapse rate ranges. Channel 2's correlation coefficients from global and polar SNOs have opposite signs. The short-term global SNO may not have sufficient temporal coverage to represent seasonal changes in low latitudes. Channels 3–6 have absolute correlation coefficients larger than 0.6 based on combined data. Similar to the N14–N15 pair, the largest correlation coefficient (0.90) is also found in channel 4. Channel 7 has relatively smaller correlation values. The nonlinear pattern in the plot partially contributes to the smaller values of linear correlation coefficients. For this channel between N17 and M02, a nonlinear approach should work better for intersatellite calibration.

Both Tables III and IV show that there is a high linear correlation between the LRF and the ISD for channel 4. This presents an opportunity to estimate channel 4's ISD from the LRF using a linear regression approach. The linear regression equations for the ISDs between N14 and N15 and between N17 and M02 are derived as

$$\mathrm{ISD}_{\mathrm{N14-N15}} = 0.400 \times \Delta\mathrm{Tb}_{\mathrm{CH5-CH4}} - 0.993 \quad (1)$$
$$\mathrm{ISD}_{\mathrm{N17}-M02} = 0.109 \times \Delta\mathrm{Tb}_{\mathrm{CH5-CH4}} - 0.287 \quad (2)$$

in which $\Delta\mathrm{Tb}_{\mathrm{CH5-CH4}}$ stands for the Tb difference between channels 5 and 4. The $\Delta\mathrm{Tb}_{\mathrm{CH5-CH4}}$ values are taken from N14 for the N14–N15 pair and taken from N17 for the N17–M02 pair. In both equations, the linear fitting coefficients are derived from all available colocated data (from both short-term global SNOs and long-term polar SNOs). Linear fitting may be also considered for other channels between certain satellite pairs that have high linear correlations, such as for channel 5 of both satellite pairs and for channel 7 of the N14–N15 pair. However, it is not recommended to use linear fitting for channels having small values of linear correlations.

TABLE IV
STATISTICS FOR MEAN OF N17–M02 ISD, MEAN OF N17 LRF, STD OF N17–M02 ISD, STD OF LRF, AND THE LINEAR CORRELATION COEFFICIENT BETWEEN LRF AND N17–M02 ISD CALCULATED BASED ON N17 AND M02 SHORT-TERM GLOBAL SNO, MULTIYEAR POLAR SNO, AND COMBINED GLOBAL AND POLAR SNO (LABELED AS "ALL") DATA FOR CHANNELS 1–7

	Channel	LRF	ISD Mean	LRF Mean	ISD STD	LRF STD	Correlation
Short-term Global	1	CH2-CH1	-1.79	-11.58	3.67	5.38	-0.606
	2	CH3-CH2	-0.83	0.27	0.65	1.32	-0.114
	3	CH4-CH3	0.10	8.90	0.51	4.23	0.393
	4	CH5-CH4	1.29	14.38	0.61	5.12	0.900
	5	CH6-CH5	-0.60	11.43	0.34	4.02	-0.813
	6	CH7-CH6	-0.10	9.85	0.30	4.02	-0.567
	7	CH8-CH7	-0.33	17.20	0.36	8.13	-0.370
Multi-year Polar	1	CH2-CH1	-2.18	-9.39	4.13	6.73	-0.461
	2	CH3-CH2	-0.59	-1.01	0.73	3.23	0.115
	3	CH4-CH3	-0.41	1.63	0.85	4.64	0.744
	4	CH5-CH4	0.35	5.99	0.49	3.61	0.747
	5	CH6-CH5	-0.20	4.18	0.32	3.28	-0.527
	6	CH7-CH6	0.22	3.32	0.37	3.21	-0.414
	7	CH8-CH7	-0.05	4.08	0.48	4.76	-0.389
All	1	CH2-CH1	-1.92	-10.83	3.84	5.96	-0.544
	2	CH3-CH2	-0.75	-0.17	0.69	2.25	-0.029
	3	CH4-CH3	-0.07	6.42	0.69	5.56	0.621
	4	CH5-CH4	0.97	11.52	0.73	6.13	0.917
	5	CH6-CH5	-0.47	8.96	0.38	5.11	-0.805
	6	CH7-CH6	0.01	7.62	0.36	4.87	-0.623
	7	CH8-CH7	-0.23	12.72	0.42	9.48	-0.457

III. SUMMARY

Global HIRS SNOs are obtained from two pairs of satellites for the time periods when their orbits overlap with each other. The first pair is for N14 and N15 during Julian Days 102–129 in 2003, and the second pair is for N17 and M02 during Julian Days 66–185 in 2009. ISDs derived from these short-term global SNOs are examined together with ISDs derived from multiyear polar SNOs. The investigation presents an observational data set for the development of intersatellite calibrations.

The examination on HIRS longwave channels shows that, for the temperature-sounding channels from lower stratosphere to lower troposphere, i.e., channels 3–7, the ISDs vary with their corresponding LRFs. The ISDs of channels 5–7 (mid- to low-tropospheric temperature channels) also vary with Tb, but this is not the case for channel 4. For this upper tropospheric channel, the ISDs are the largest in low latitudes, where the values of both LRF and Tb are large. However, the ISDs in high latitudes are much smaller for similarly large Tb values due to a much smaller LRF there. The difference in ISD patterns in low latitudes and high latitudes produces a fork feature in channel-4 Tb scatter plots between overlapping satellites. A fork feature also appears in the channel-4 scatter plot between the ISD and the brightness temperature. The upper tropospheric water-vapor channel 12 between N14 and N15 displays a large ISD due to a large change in the channel frequency. The low-latitude SNO reveals ISD values as large as 12 K in channel 12, which is a value much larger than what can be covered by the polar SNO.

The HIRS measurements on two pairs of satellites examined in this paper exhibit the instrument design transitions from HIRS/2 to HIRS/3 and from HIRS/3 to HIRS/4. In the transition from HIRS/2 to HIRS/3, a couple of channels experienced relatively larger ISDs compared with channels in the same designs [3]. A significant ISD occurs in channel 12 between HIRS/2 and HIRS/3. The ISD in channel 4 between HIRS/2 and HIRS/3 is larger than the ISDs within HIRS/2 and HIRS/3. The ISD in channel 4 between HIRS/3 and HIRS/4 is also slightly larger than the ISDs within HIRS/3. For other channels, from the comparisons with polar SNOs presented in [3], the ISD values between instrument design transitions are not found to be significantly larger than those between satellite pairs in the same designs. Some channels, such as channel 10, underwent larger spectral changes within HIRS/2 design than spectral changes from HIRS/2 to HIRS/3. The unique features of channel-4 ISDs revealed from low-latitude observations are expected to exist in all other satellite pairs, although the significance of the fork features in Tb-versus-Tb scatter plots and ISD-versus-Tb scatter plots can differ from satellite pairs to satellite pairs. The fork features are the result of the unique combination of warm temperatures coupled with small lapse rates in high latitudes in upper troposphere during parts of the year in contrast to the warm temperatures coupled with large lapse rates in low latitudes.

During the brief periods when two polar orbiting satellites come close to each other, it gives us a glimpse of ISD on a global scale. The brief global view fills a large gap in quantifying ISDs over low latitudes. However, such short-term instances cannot replace long-term observations. Comparisons between ISDs derived from global and polar SNOs show that the approaches of using global SNOs and polar SNOs to infer ISDs have their own advantages and limitations. Global SNOs provide a large dynamical range of the Tb observation, particularly for tropospheric channels. Without observations from low latitudes, the fork features of channel 4, as shown in Figs. 1 and 3, would not have been revealed. However, two polar orbiting satellites overlap for only a short time. Within

the limited time frame, seasonal changes in the stratosphere and the upper troposphere are not captured by the short-term global SNOs. On the other hand, based on years of observation, polar SNO typically records a wider range of Tb measurements in the stratosphere and provides a good representation in the lower end of Tb measurements in the troposphere. However, due to geographical limitation of polar SNOs, ISDs associated with high temperatures in the mid- to low troposphere and in the water-vapor channels are not covered by this data set. One needs to keep in mind these data limitations, and whenever possible, long-term and global coverages should be both used to infer a fuller picture of the ISD.

ACKNOWLEDGMENT

The author would like to thank C. Cao and L. Wang of the Center for Satellite Applications and Research for providing the polar simultaneous-nadir-overpass-observation data; D. Jackson of the Cooperative Institute for Research in Environmental Sciences, University of Colorado/National Oceanic and Atmospheric Administration Earth System Research Laboratory, for providing the High-Resolution Infrared Radiation Sounder cloud-clearing code; and the two anonymous reviewers for helpful comments and suggestions.

REFERENCES

[1] J. J. Bates, X. Wu, and D. L. Jackson, "Interannual variability of upper-troposphere water vapor band brightness temperature," *J. Climate*, vol. 9, no. 2, pp. 427–438, Feb. 1996.

[2] C. Cao, H. Xu, J. Sullivan, L. McMillin, P. Ciren, and Y.-T. Hou, "Intersatellite radiance biases for the high-resolution infrared radiation sounders (HIRS) on board NOAA-15, -16, and -17 from simultaneous nadir observations," *J. Atmos. Ocean. Technol.*, vol. 22, no. 4, pp. 381–395, Apr. 2005.

[3] L. Shi, J. J. Bates, and C. Cao, "Scene radiance–dependent intersatellite biases of HIRS longwave channels," *J. Atmos. Ocean. Technol.*, vol. 25, no. 12, pp. 2219–2229, Dec. 2008.

[4] L. Wang, C. Cao, and P. Ciren, "Assessing NOAA-16 HIRS radiance accuracy using simultaneous nadir overpass observations from AIRS," *J. Atmos. Ocean. Technol.*, vol. 24, no. 9, pp. 1546–1561, Sep. 2007.

[5] C. Cao, M. Goldberg, and L. Wang, "Spectral bias estimation of historical HIRS using IASI observations for improved fundamental climate data records," *J. Atmos. Ocean. Technol.*, vol. 26, no. 7, pp. 1378–1387, Jul. 2009.

[6] L. Shi and J. J. Bates, "Three decades of intersatellite-calibrated high-resolution infrared radiation sounder upper tropospheric water vapor," *J. Geophys. Res.*, vol. 116, no. D4, p. D04 108, Feb. 22, 2011.

[7] M. Goldberg, G. Ohring, J. Butler, C. Cao, R. Datla, D. Doelling, V. Gartner, T. Hewison, B. Iacovazzi, D. Kim, T. Kurino, J. Lafeuille, P. Minnis, D. Renaut, J. Schmetz, D. Tobin, L. Wang, F. Weng, X. Wu, F. Yu, P. Zhang, and T. Zhu, "The global space-based inter-calibration system," *Bull. Amer. Meteorol. Soc.*, vol. 92, no. 4, pp. 467–475, Apr. 2011.

[8] V. O. John, G. Holl, S. A. Buehler, B. Candy, R. W. Saunders, and D. E. Parker, "Understanding intersatellite biases of microwave humidity sounders using global simultaneous nadir overpasses," *J. Geophys. Res.*, vol. 117, no. D2, p. D02 305, Jan. 28, 2012.

[9] A. Chedin, E. Pequignot, S. Serrar, and N. A. Scott, "Simultaneous determination of continental surface emissivity and temperature from NOAA 10/HIRS observations: Analysis of their seasonal variations," *J. Geophys. Res.*, vol. 109, no. D20, p. D20 110, Oct. 19, 2004.

[10] L. Shi, G. Peng, and J. J. Bates, "Surface air temperature and humidity from intersatellite-calibrated HIRS measurements in high latitudes," *J. Atmos. Ocean. Technol.*, vol. 29, no. 1, pp. 3–13, Jan. 2012.

[11] B. Ruston, F. Weng, and B. Yan, "Use of a one-dimensional variational retrieval to diagnose estimates of infrared and microwave surface emissivity over land for ATOVS sounding instruments," *IEEE Trans. Geosci. Remote Sens.*, vol. 46, no. 2, pp. 393–402, Feb. 2008.

[12] D. P. Wylie and W. P. Menzel, "Eight years of high cloud statistics using HIRS," *J. Climate*, vol. 12, no. 1, pp. 170–184, Jan. 1999.

[13] D. Wylie, D. L. Jackson, W. P. Menzel, and J. J. Bates, "Trends in global cloud cover in two decades of HIRS observations," *J. Climate*, vol. 18, no. 15, pp. 3021–3031, Aug. 1, 2005.

[14] D. Wylie, E. Eloranta, J. D. Spinhirne, and S. P. Palm, "Comparison of cloud cover statistics from the GLAS lidar with HIRS," *J. Climate*, vol. 20, no. 19, pp. 4968–4981, Oct. 2007.

[15] H. T. Lee, A. Gruber, R. G. Ellingson, and I. Laszlo, "Development of the HIRS outgoing longwave radiation climate dataset," *J. Atmos. Ocean. Technol.*, vol. 24, no. 12, pp. 2029–2047, Dec. 2007.

[16] E. Fishbein, C. B. Farmer, S. L. Granger, D. T. Gregorich, M. R. Gunson, S. E. Hannon, M. D. Hofstadter, S. Y. Lee, S. S. Leroy, and L. L. Strow, "Formulation and validation of simulated data for the Atmospheric Infrared Sounder (AIRS)," *IEEE Trans. Geosci. Remote Sens.*, vol. 41, no. 2, pp. 314–329, Feb. 2003.

[17] W. B. Rossow and L. C. Garder, "Cloud detection using satellite measurements of infrared and visible radiances for ISCCP," *J. Climate*, vol. 6, no. 12, pp. 2341–2369, Dec. 1993.

[18] D. L. Jackson, D. P. Wylie, and J. J. Bates, "The HIRS pathfinder radiance data set (1979–2001)," in *Proc. 12th Conf. Satellite Meteorol. Ocean.*, Long Beach, CA, 2003, pp. 1–4.

[19] C. Cao, M. Weinreb, and H. Xu, "Predicting simultaneous Nadir overpasses among polar-orbiting meteorological satellites for the intersatellite calibration of radiometers," *J. Atmos. Ocean. Technol.*, vol. 21, no. 4, pp. 537–542, Apr. 2004.

[20] Y. Kuroda, "Effect of stratospheric sudden warming and vortex intensification on the tropospheric climate," *J. Geophys. Res.—Atmos.*, vol. 113, no. 15, p. D15 110, Aug. 5, 2008.

[21] C. Stan and D. M. Straus, "Stratospheric predictability and sudden stratospheric warming events," *J. Geophys. Res.*, vol. 114, no. D12, p. D12 103, Jun. 17, 2009.

[22] S. M. Deng, Y. J. Chen, Y. Huang, T. Luo, and Y. Bi, "Transient characteristics of residual meridional circulation during stratospheric sudden warming," *Adv. Atmos. Sci.*, vol. 28, no. 3, pp. 551–563, May 2011.

[23] L. P. Bobylev, E. V. Zabolotskikh, L. M. Mitnik, and M. L. Mitnik, "Arctic polar low detection and monitoring using atmospheric water vapor retrievals from satellite passive microwave data," *IEEE Trans. Geosci. Remote Sens.*, vol. 49, no. 9, pp. 3302–3310, Sep. 2011.

[24] K. R. Knapp, "Inter-satellite bias of the high resolution infrared radiation sounder water vapor channel determined using ISCCP B1 data," *J. Appl. Remote Sens.*, vol. 6, no. 1, p. 063523, Mar. 2012.

[25] Y. Harada, A. Goto, H. Hasegawa, N. Fujikawa, H. Naoe, and T. Hirooka, "A major stratospheric sudden warming event in January 2009," *J. Atmos. Sci.*, vol. 67, no. 6, pp. 2052–2069, Jun. 2010.

[26] K. Yoshida and K. Yamazaki, "Tropical cooling in the case of stratospheric sudden warming in January 2009: Focus on the tropical tropopause layer," *Atmos. Chem. Phys.*, vol. 11, no. 13, pp. 6325–6336, Jul. 2011.

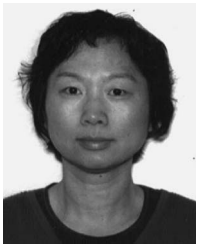

Lei Shi received the B.S. degree in meteorology from Zhongshan University, Guangzhou, China, in 1984 and the M.S. and Ph.D. degrees in meteorology from Florida State University, Tallahassee, in 1989 and 1992, respectively.

She is a Meteorologist with the National Climatic Data Center, National Oceanic and Atmospheric Administration, Asheville, NC. Her current research interests include High-Resolution Infrared Radiation Sounder (HIRS) intersatellite calibration, variability of HIRS upper tropospheric water vapor, HIRS retrieval of temperature and humidity profiles, and Advanced Microwave Sounding Unit retrieval of sea surface air temperature and humidity.

Dr. Shi is a member of the American Meteorological Society and the American Geophysical Union.